J. Plasma Physics (1997), *vol.* 58, *part* 3, *pp.* 455–466. Printed in the United Kingdom
© 1997 Cambridge University Press

Plasma sheath evolution from perturbed electrodes in a negative-ion plasma. Part 2. Experiment and PIC simulation

SEUNGJUN YI,[1] YASSER EL-ZEIN,[2]
KARL E. LONNGREN[1,2] and TERENCE E. SHERIDAN[3]

[1] Department of Physics and Astronomy and [2] Department of Electrical and Computer Engineering, The University of Iowa, Iowa City, Iowa 52242, USA
[3] Department of Physics, West Virginia University, Morgantown, West Virginia 26506-6315, USA

(Received 3 September 1996)

The two-dimensional spatial and temporal evolution of a plasma surrounding an electrode whose potential is suddenly decreased is experimentally investigated. The electrode contains a localized convex or a localized concave perturbation. The quasineutral plasma consists of positive ions and various proportions of negative ions and electrons. The results are compared and contrasted with those that are obtained numerically using a particle-in-cell (PIC) simulation and those that had previously been obtained using a fluid-model code.

1. Introduction

In a previous paper (El-Zein *et al.* 1997), we described the temporal and spatial plasma evolution from a metal electrode that was inserted in an unmagnetized homogeneous two- or three-component quasineutral plasma and to which a negative step voltage had been applied. Negative ions form the third component in the latter plasma, and we call such a plasma a *negative-ion plasma*. In that investigation, we studied the additional effects that would be introduced owing to the addition of a localized convex or concave perturbation to a flat electrode. We modelled the perturbation in the electrode with a local perturbation in the applied voltage signal. The results of the plasma evolution were obtained using a two-dimensional fluid-model code that we had used previously to study the plasma evolution from 90° convex or concave metal electrodes (El-Zein *et al.* 1996).

The general conclusions obtained in those simulations were that the electrons would initially be expelled into the uniform ambient plasma before either species of the more massive ions would have a chance to move. This creates a localized region of net positive charge adjacent to the electrode. This local region of charge non-neutrality adjacent to the pulsed electrode has been given the name *transient sheath* or *ion-matrix sheath*. In preliminary experiments, it was suggested that this sheath tended to pull away from a concave corner and would crowd around a convex corner (Lim *et al.* 1991). This was in agreement with a related numerical study of the sheath (Donnelly and Watterson 1989). As time increases, the positive ions adjacent to the electrode would be absorbed

https://doi.org/10.1017/S0022377897006065 Published online by Cambridge University Press

by it, causing the front of a rarefactive positive-ion sheath to expand into the plasma with a velocity that is initially greater than the fast-mode ion acoustic velocity in the negative-ion plasma. The expanding sheath slows down to this velocity. Negative ions will be repelled by the negative potential applied to the electrode, and these ions will also expand into the plasma. An extended list of related references appears in these two papers that are based on a collisionless fluid-model simulation (El-Zein *et al.* 1996, 1997).

A numerical simulation based on a 'collisionless' fluid model suffers from collisionality whenever the trajectories of fluid elements converge or intersect (Sheridan 1996*a*). This is unavoidable in two and three dimensions. Furthermore, fluid equations are moment equations, and therefore may not adequately represent the distribution function at each point in space. Consequently, to model the experiments presented in this paper, we develop a particle-in-cell (PIC) simulation (Birdsall and Langdon 1991). In such a model, ion particles are effectively collisionless, while the velocity distribution is represented by a number of ion particles with differing velocities. Our model is an extension of a PIC model used to explore two-dimensional problems in pulsed sheath expansion (Sheridan 1996*a–c*), especially problems relevant to plasma-based ion implantation. We show that our model gives results in good agreement with experiment, providing us with the confidence to take a more detailed look at the physics of this phenomenon using the simulation.

In the present investigation, we describe a series of laboratory experiments that were designed to verify the conclusions that were suggested in the above fluid-model simulations. the electrode perturbation, in this case, will be in the physical construction rather than in the applied voltage signal, as was previously used. In addition, a PIC simulation will be used to extend the investigation to gain an understanding of the effects of the individual species of particle. Four electrodes are simulated in the calculation:

(*a*) a 90° concave corner;

(*b*) a 90° convex corner;

(*c*) a flat electrode containing a concave perturbation;

(*d*) a flat electrode containing a convex perturbation.

The experimental setup is described in Sec. 2. Section 3 summarizes the results that were obtained from the laboratory experiments. The results of the PIC simulation are in Sec. 4. Concluding comments are given in Sec. 5.

2. Experimental setup

The experiments were performed in a large multidipole plasma device that has been described elsewhere (Cooney *et al.* 1993; Aossey *et al.* 1993). The device consists of several hollow rectangular tubes that were filled with approximately 1500 small permanent magnets. Each row had magnet pole faces pointing in the same direction, and the rows alternated in magnetic pole orientation. The tubes were arranged in a cage structure (80 cm diameter $\times$ 110 cm length), and the entire structure was inserted in a large vacuum chamber whose base vacuum pressure was maintained beneath 10^{-6} Torr by continuous pumping. Argon was bled into the chamber to maintain a neutral pressure of $1–2 \times 10^{-4}$ Torr using

https://doi.org/10.1017/S0022377897006065 Published online by Cambridge University Press

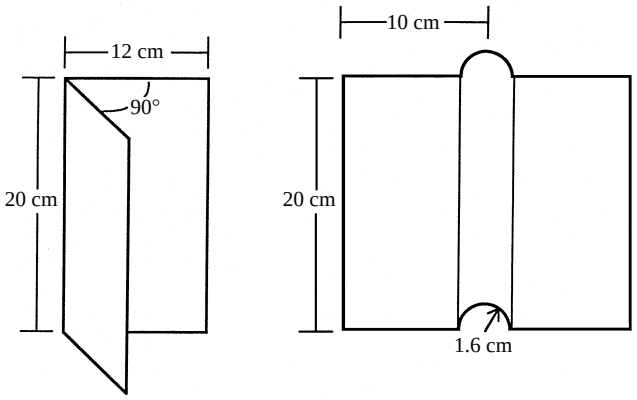


Figure 1. Experimental electrodes: (*a*) a 90° corner; (*b*) electrode with a cylindrical perturbation.

a double-valve system. One valve was used to control the pressure, and the second was an 'open–close' valve. Ionizing electrons emitted from Joule-heated filaments were accelerated by an 85 V bias supply to the cage, which served as the anode. Typical plasma numbers as monitored with a Langmuir probe were electron density $n_e \approx 10^8$–10^9 cm^{-3} and electron temperature $T_e \approx 1$–3 eV. The ion temperature T_i was $T_i < \frac{1}{10}T_e$. The plasma potentials ranged from $+12$ V to $+2$ V, and decreased as the amount of SF_6 was increased. The plasma was quiet, and the small amount of noise present decreased with the addition of the SF_6. The plasma was also relatively homogeneous in the region of the experiment.

The percentage of SF_6 was estimated in two ways. First, as a crude estimate, the pressure of neutral SF_6 in the evacuated chamber was set to be a certain percentage of the known value of Ar prior to the opening of the Ar-gas valve. The second technique involved monitoring the reduction of the election saturation current of the Langmuir probe. We define a parameter ε, the negative-ion concentration, to be

$$\varepsilon = \frac{n_{SF_6^-}}{n_{Ar^+}} = \frac{n_{Ar^+} - (n_{Ar^+} - n_{SF_6^-})}{n_{Ar^+}} = 1 - \frac{I_{es}}{I_{es}^{(0)}}, \tag{1}$$

where I_{es} and $I_{es}^{(0)}$ are the Langmuir probe saturation currents with and without the SF_6. Other negative ions such as SF_5^- and F^- may have also been present in the device. Their presence will not alter the conclusions that are reached in this work, so no effort was made to quantify their amounts.

Waves were excited by applying a voltage signal to one of the two copper launchers depicted in Fig. 1. The first launcher was a 90° copper corner, shown in Fig. 1 (*a*). The second launcher was a flat copper sheet containing a cylindrical perturbation, shown in Fig. 1 (*b*). Both launchers could be rotated by 180°. Hence it was possible to examine effects due to concave and convex launchers. The amplitude $\Delta\phi$ of the applied voltage signal was $\Delta\phi \approx -9$ V. The repetition frequency of the voltage step was ≈ 5000 Hz.

All signals were detected with a 3 mm diameter spherical Langmuir probe that was biased positive with respect to the plasma potential in order to detect

https://doi.org/10.1017/S0022377897006065 Published online by Cambridge University Press

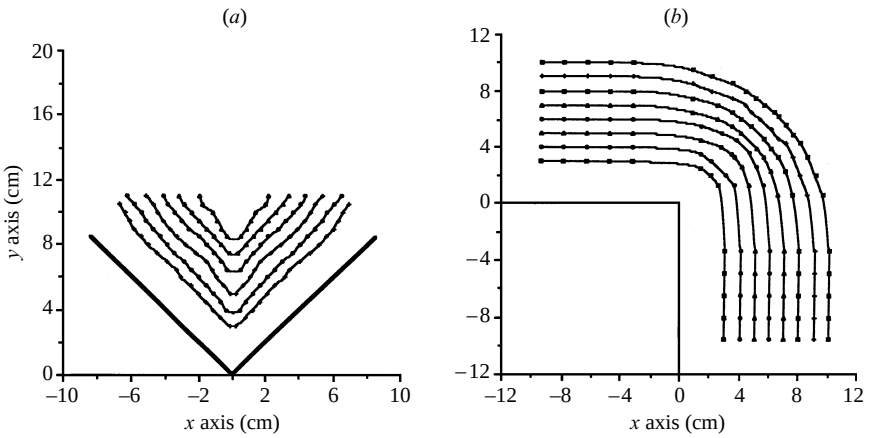


Figure 2. Measured equiphase contours from the 90° concave and the 90° convex launchers. The solid lines represent the metallic surfaces. (*a*) Concave launcher; contours begin at $t = 5\ \mu$s and increase in steps of $\Delta t = 3\ \mu$s to $t = 20\ \mu$s. (*b*) Convex launcher; contours begin at $t = 6.3\ \mu$s and increase in steps of $\Delta t = 2.6\ \mu$s to $t = 24.5\ \mu$s.

perturbations in the electron saturation current. The probe could be scanned in the entire region in front of the launching structures. The perturbations in current were passed through a resistor to ground, and the resulting voltage perturbations were displayed on a digital oscilloscope and stored in a computer. The signal generator provided the necessary triggering signals.

3. Experimental results

The measured equiphase contours from the 90° concave electrode and the convex electrode are presented in Fig. 2. In our experiment, we define an equiphase contour as the leading edge of a negative-potential pulse launched by the electrode. The contours of the concave electrode begin at $t = 5\ \mu$s and increase by steps of $\Delta t = 3\ \mu$s to $t = 20\ \mu$s, and those of the convex electrode begin at $t = 6.3\ \mu$s and increase by steps of $\Delta t = 2.6\ \mu$s to $t = 24.5\ \mu$s. The solid lines in Fig. 2 represent the electrode surfaces. It is noted in our experimental results that the measured equiphase contours are pushed away and separate from the corner of the concave electrode, while they are pushed in and crowd around the corner of the convex electrode. This is in accordance with our simulation using the fluid equations (El-Zein *et al.* 1996).

As can be seen in Fig. 2(*b*), the contours around the convex corner seem to be cylindrical in shape. It was suggested in the simulation that the corner of a convex electrode appears to be similar to a cylindrical electrode. To check this prediction, we measured the spatial dependence of the amplitude of the wave along the 45° line. The amplitude dependence as a function of distance is depicted in Fig. 3. We ascertained that the cylindrically expanding wave had one property of a cylindrical soliton that was launched from the corner. We include a line to represent the geometrical decay of a cylindrical soliton (amplitude $\approx r^{-2/3}$) (Das and Singh 1991; Williams *et al.* 1992). No other soliton characteristics were examined in this experiment. We have previously been able to observe several KdV and mKdV soliton properties in this plasma (Cooney *et al.* 1993; Yi *et al.* 1996).

https://doi.org/10.1017/S0022377897006065 Published online by Cambridge University Press

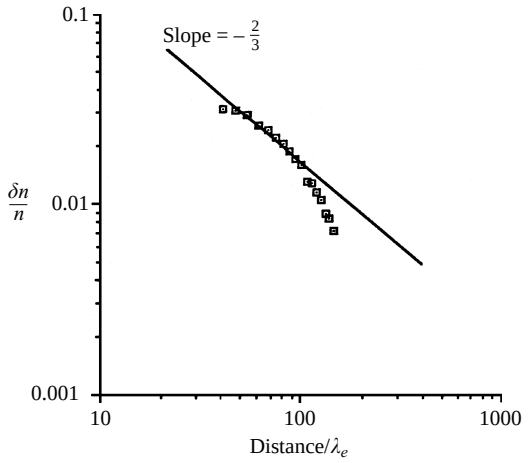


Figure 3. Amplitude dependence as a function of distance (normalized by the electron Debye length λ_e). The solid line represents the geometrical amplitude decay of a cylindrical soliton.

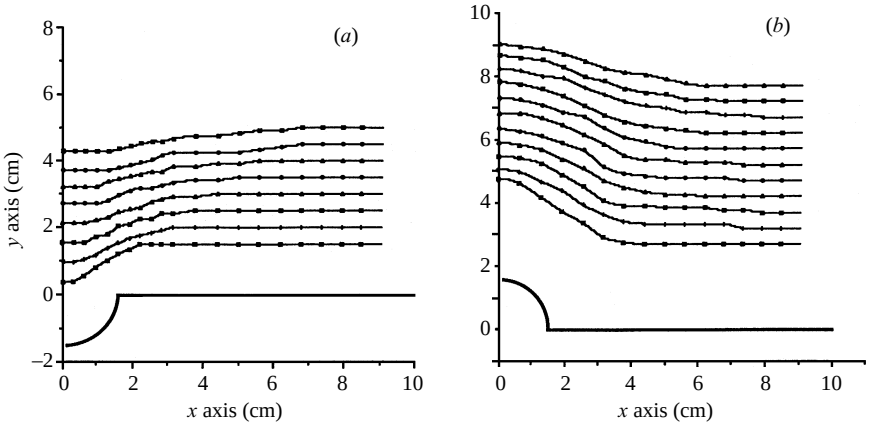


Figure 4. Measured equiphase contours from the flat launchers with cylindrical concave and convex perturbations. The solid lines represent the metallic surfaces. (*a*) Concave perturbation; contours begin at $t = 3.2\ \mu$s and increase in steps of $\Delta t = 1.5\ \mu$s to $t = 13.7\ \mu$s. (*b*) Convex perturbation; contours begin at $t = 6.5\ \mu$s and increase in steps of $\Delta t = 1.3\ \mu$s to $t = 19.5\ \mu$s.

The measured equiphase contours from the electrodes with a concave perturbation and a convex perturbation are shown in Fig. 4. The contours of the electrode with a concave perturbation begin at $t = 3.2\ \mu$s and increase in equal increments of $\Delta t = 1.5\ \mu$s to $t = 13.7\ \mu$s, and those of the electrode with a convex perturbation begin at $t = 6.5\ \mu$s and increase in equal increments of $\Delta t = 1.3\ \mu$s to $t = 19.5\ \mu$s. The first contours of both electrodes are similar to the actual surface of the electrode in shape, but appear to expand transversely. For the electrode with a concave perturbation, the contours are pushed away at the concave portion, while they are pushed in at the convex corner joining the concave perturbation to the flat electrode. A similar interpretation can be given to the electrode with a convex perturbation. As both contours expand from the electrodes, they flatten and are essentially planar far from the electrodes. This

https://doi.org/10.1017/S0022377897006065 Published online by Cambridge University Press

was noted in the experiments using in the 90° corners. This is also in qualitative agreement with a simulation using the fluid equations (El-Zein *et al.* 1997).

4. Particle-in-cell simulation

The PIC model is first described. We then compare the results of the PIC simulation with the laboratory experiment. We finally use the PIC simulation to predict additional plasma properties.

4.1. Model

We consider a negative-ion plasma containing positive ions, negative ions and electrons. The charge and mass of the positive ions are $+e$ and M_+, and those of the negative ions are $-e$ and M_-. The plasma is in contact with a flat plate with a concave cylindrical perturbation of radius R as shown in Fig. 1. We assume that the densities of the three components are initially spatially uniform, with an electron density n_{e0}, a positive-ion density n_{+0}, and a negative-ion density n_{-0}. Initially, the plasma is charge-neutral, so that

$$n_{+0} - n_{-0} - n_{e0} = 0, \tag{2}$$

and the plasma and electrode are at a potential $V = 0$. At time $t = 0$, the potential on the electrode is driven to a negative excitation voltage $V_{\rm ex}$ with a rise time t_r, attracting positive ions and repelling both negative ions and electrons. The positive-ion density n_+, the negative-ion density n_-, the electron density n_e and the potential V then evolve self-consistently.

We model this situation using cold, unmagnetized, collisionless particle ions, Boltzmann electrons with a temperature T_e, and the Poisson equation. In dimensionless units, the Poisson equation is

$$\nabla^2\phi = -(\tilde{n}_+ - \tilde{n}_- - e^{\phi}), \tag{3}$$

while the equations of motion for positive and negative ions are

$$\frac{d^2\mathbf{X}}{d\tau^2} = -\nabla\phi, \tag{4a}$$

$$\frac{d^2\mathbf{X}}{d\tau^2} = \frac{1}{\mu}\nabla\phi \tag{4b}$$

respectively, and the charge-neutrality condition (2) becomes

$$\tilde{n}_{+0} - \tilde{n}_{-0} - 1 = 0. \tag{5}$$

Here the dimensionless variables are

$$\mathbf{X} = \frac{\mathbf{x}}{\lambda_e}, \quad \tau = t\omega_{pi}, \quad \phi = \frac{eV}{\kappa_B T_e}, \quad \tilde{n}_+ = \frac{n_+}{n_{e0}}, \quad \tilde{n}_- = \frac{n_-}{n_{e0}}, \tag{6}$$

where $\lambda_e = (\varepsilon_0 \kappa T_e / n_{e0} e^2)^{1/2}$ is the Debye length, and $\omega_{pi} = (n_{e0} e^2/\varepsilon_0 M_+)^{1/2}$ is the positive-ion plasma frequency. The parameter $\varepsilon = n_{-0}/n_{+0}$ gives the relative negative-ion density, while the mass ratio is given by $\mu = M_-/M_+$ and the dimensionless excitation voltage is $\phi_{\rm ex} = eV_{\rm ex}/\kappa_B T_e$.

The model is solved using a particle-in-cell PIC simulation (Birdsall and Langdon 1991). At each time, the gradient of the potential (i.e. the electric field) is used to advance the ion positions (4). The density of each ion species is then

https://doi.org/10.1017/S0022377897006065 Published online by Cambridge University Press

calculated on a grid, and the nonlinear Poisson equation (3) is solved iteratively for the potential. These steps are then repeated a number of times.

As described above, for the concave perturbation the experimental parameters were $n_{e0} = 1.4 \times 10^8$ cm^{-3}, $T_e = 1.2$ eV, $\varepsilon = 0.52$ and $V_{\rm ex} = -9.0$ V, and the radius of the perturbation was $R = 1.6$ cm. The positive-ion species was Ar^+, and the dominant negative species was SF_6^-. From these values, we calculate the following parameters: $\mu = 3.66$, $\lambda_e = 0.069$ cm, $\omega_{pi} = 2.5 \times 10^6$ s^{-1} and $\phi_{\rm ex} = -7.50$ (assuming that the plasma potential is approximately zero), and the radius of the perturbation is $23.2\lambda_e$. In addition, we use a time step $\Delta t = \frac{1}{32}\omega_{pi}^{-1}$ and a rise time $t_r = \frac{1}{16}\omega_{pi}^{-1}$. Using a fast ($t_r \ll \omega_{pi}^{-1}$) but non-zero rise time gets the simulation off to a smooth start. The simulation box was symmetric about $x = 0$, and extended $144\lambda_e$ in the x direction, $112\lambda_e$ in the positive y direction and $24\lambda_e$ in the negative y direction, as required to encompass the concave perturbation. The grid spacing was λ_e in both the x and y directions. Particles encountering the $x = 0$ symmetry plane were reflected back into the simulation box. Initially 36 positive-ion and 36 negative-ion particles were placed in each cell, so that the simulation began with about 6000000 particles of each species.

4.2. Comparison of experimental and PIC simulation results

The primary point of comparison between the experiment and the model is the time dependence of the position of the leading edge of the pulse launched by the electrode. For the simulation, we choose this as the line on which the electron density has fallen to one-half of its ambient plasma value (i.e. $e^{\phi} = 0.5$). This is shown in Fig. 5(*a*) for the concave perturbation and in Fig. 5(*b*) for the convex perturbation. The axes are labelled using both dimensional and dimensionless variables. Qualitative agreement with the experimental results shown in the respective plots in Fig. 4 is good. First note that, at early times, the pulse edge conforms closely to the electrode. Far from the perturbation, the pulse is essentially planar, and propagates with constant speed. The concave portion of the pulse expands more rapidly, causing the pulse to become increasingly linear. Further, the concave portion of the pulse expands laterally (in the x direction), so that eventually the concave part flattens, as also seen in the experimental data. However, in comparison to the experiment, we see that the simulated pulse speed is greater than that measured, probably indicating that the experimentally reported value of ε is slightly too large. In addition, the depth of the pulse above the perturbation is somewhat smaller than seen experimentally, which may be due to neglect of the presheath, or to an underestimate of the plasma density.

In Fig. 5(*b*), we plot the position of the leading edge of the pulse for the convex perturbation as predicted by the PIC simulation. From the experimental values, we calculate the following simulation parameters; $\lambda_e = 0.055$ cm, $\omega_{pi} = 3.4 \times 10^6$ s^{-1} and $\phi_{\rm ex} = -6.0$, and the radius of the perturbation is $29\lambda_e$. Because of the greater ion plasma frequency in this case, we ran the simulation to $t\omega_{pi} = 40$ (11.8 μs), which is somewhat less than the time for which experimental results are available. In the experimental data, we see that the convex part of the pulse propagates more slowly than the planar part, while spreading laterally. Similar features are seen in the simulation results, with the following important exception. In the simulation, the portion of the pulse

https://doi.org/10.1017/S0022377897006065 Published online by Cambridge University Press

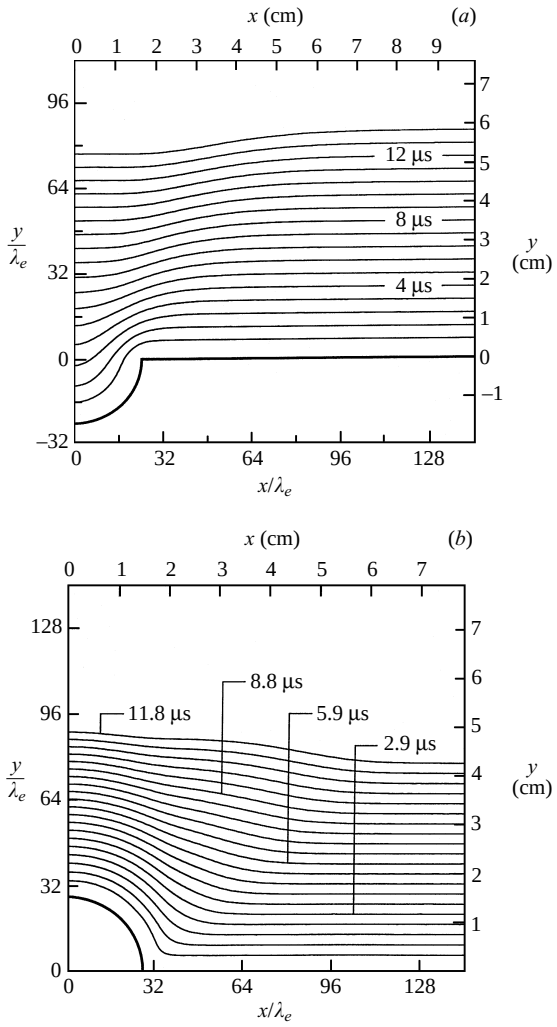


Figure 5. Position of the leading edge of the pulse versus time as computed by the particle-in-cell (PIC) simulation. The heavy line represents the electrode surface. The x and y axes are labelled with both dimensionless and dimensional units. (*a*) Concave launcher; contours begin at $t = 0.8\ \mu$s ($2\omega_{pi}^{-1}$) and increase in steps of $\Delta t = 0.8\ \mu$s ($2\omega_{pi}^{-1}$) to $t = 13.6\ \mu$s ($34\omega_{pi}^{-1}$). (*b*) Convex launcher; contours begin at $t = 0.294\ \mu$s ($2\omega_{pi}^{-1}$) and increase in steps of $\Delta t = 0.294\ \mu$s ($2\omega_{pi}^{-1}$) to $t = 11.85$ s ($40\omega_{pi}^{-1}$).

launched from the interior corner (where the perturbation joins the plane) is largest, and therefore has the greatest speed. Thus this portion eventually overtakes the other parts, creating a small perturbation in the pulse front above, and to the right of, the interior corner. This feature is not seen in the experimental data, possibly because the density in the corner is below the ambient plasma value, violating the assumption of an initially uniform plasma.

4.3. Predictions from the PIC simulation

That we find good agreement between the experiment and simulation using experimentally measured parameters gives us some confidence that the model captures the important physics in this problem. With this assurance, we can

https://doi.org/10.1017/S0022377897006065 Published online by Cambridge University Press

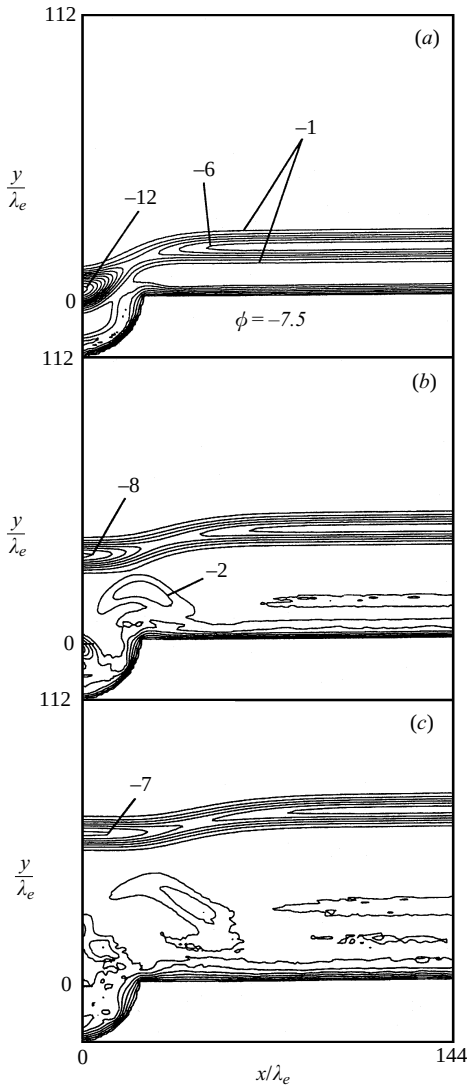


Figure 6. Equipotentials for the non-dimensional potential $\phi = V/(\kappa_B T_e/e)$ for times (*a*) $t = 4.0\,\mu$s $(10\omega_{pi}^{-1})$, (*b*) $8.0\,\mu$s $(20\omega_{pi}^{-1})$ and (*c*) $12\,\mu$s $(30\omega_{pi}^{-1})$. The x and y axes are non-dimensionalized using the electron Debye length λ_e. Contours begin at $\phi = -1$ and continue downwards in steps of -1. The electrode potential is $\phi = -7.5$. The pulse created when the electrode was driven negative is seen propagating into the ambient plasma.

then use the model to explore the microphysics of this problem. In addition, the model can predict quantities that are difficult to measure or to explore parameter regimes that are inaccessible experimentally. In the following, we shall present results using the concave perturbation only.

In Fig. 6, we display the time evolution of the dimensionless potential ϕ for $t = 4$, 8 and 12 μs (10, 20 and 30 ω_{pi}^{-1}). The negative-potential pulse launched from the electrode is seen propagating into the plasma. Far from the perturbation, the pulse is essentially planar, while near the perturbation it is concave. The planar pulse appears to be symmetric from front to back, and the

https://doi.org/10.1017/S0022377897006065 Published online by Cambridge University Press

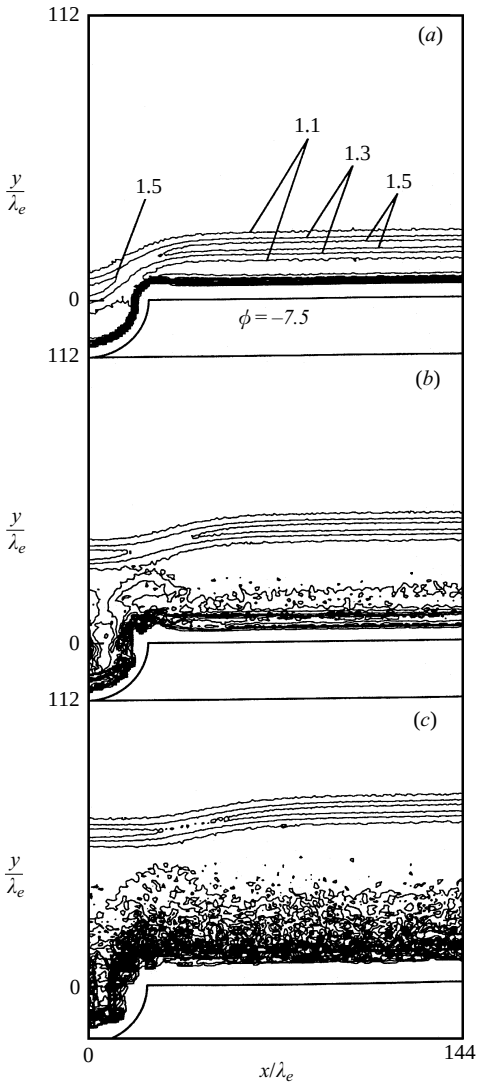


Figure 7. Contours of normalized negative-ion density at times (*a*) $t = 4.0\ \mu$s ($10\omega_{pi}^{-1}$), (*b*) $8.0\ \mu$s ($20\omega_{pi}^{-1}$) and (*c*) $12\ \mu$s ($30\omega_{pi}^{-1}$). In the ambient plasma, the normalized density is one. Negative ions are compressed by the pulse.

change in potential across the pulse is approximately zero. In the two later frames (Figs 6*b*, *c*), the launching of a smaller pulse obliquely to the electrode is also seen.

In Fig. 7, we plot contours of normalized negative-ion density. Here the value of the density in the plasma (far from the electrode) is taken to be one. At $t = 4\ \mu$s ($10\omega_{pi}^{-1}$), we see that the negative ions have been pushed away from the electrode by the transient or ion-matrix sheath, so that the negative-ion density near the electrode is zero. Negative ions do, however, bunch together near the sheath edge. The pulse is just visible as it moves away from the electrode, and part of it is still inside the concavity. The negative-ion density increases above ambient in the pulse – negative ions are compressed by the pulse. By $t = 8\ \mu$s

https://doi.org/10.1017/S0022377897006065 Published online by Cambridge University Press

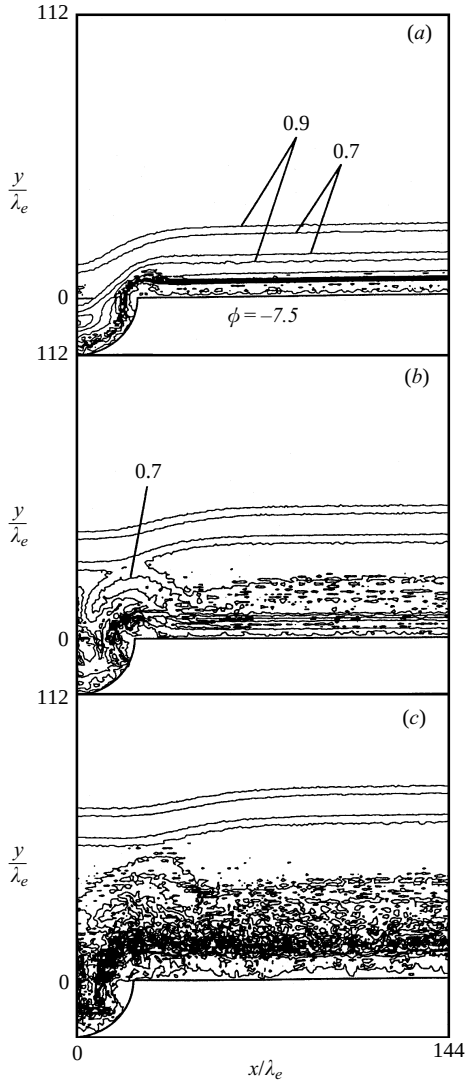


Figure 8. Contours of normalized positive-ion density at times (*a*) $t = 4.0\,\mu$s ($10\omega_{pi}^{-1}$), (*b*) $8.0\,\mu$s ($20\omega_{pi}^{-1}$) and (*c*) $12\,\mu$s ($30\omega_{pi}^{-1}$). The normalized density is one in the ambient plasma. Positive ions are rarefacted by the pulse.

($20\omega_{pi}^{-1}$), the pulse has clearly separated from the electrode, and has begun to straighten. In addition, it appears that the sheath edge is becoming unstable near the corner. At $t = 12\,\mu$s ($30\omega_{pi}^{-1}$), we see the pulse propagating serenely away from the electrode, while the density becomes increasingly noisy near the electrode. This noise is due to the growth of short-wavelength instabilities out of the initial particle noise.

In Fig. 8, we show contours of normalized positive-ion density. We see that the positive-ion density decreases in the pulse – the pulse rarefacts the positive ions. In a frame moving with the pulse, the positive ions are flowing across a potential well. Consequently, as they gain speed falling into the potential well, their density decreases because of continuity. As they slow again upon exiting

https://doi.org/10.1017/S0022377897006065 Published online by Cambridge University Press

from the well, the positive-ion density increases, and finally (nearly) regains its ambient plasma value, since the total potential drop across the pulse is approximately zero. In addition, we see the positive ions streaming across the sheath towards the electrode. They are, however, held back by the negative ions bunched together at the sheath edge. That is, in order to draw positive ions to the electrode, negative ions must also be removed from the sheath area to maintain charge neutrality.

5. Conclusion

The two-dimensional plasma evolution from pulsed nonplanar electrodes has been investigated in a negative-ion plasma. Laboratory experiments are in good agreement with the present PIC simulation and a previous fluid-model simulation.

References

Aossey, D., Amin, A., Cooney, J. L., Kim, H. S., Nguyen, B. T. and Lonngren, K. E. 1993 Variations of plasma parameters in unmagnetized and magnetized argon–SF_6–electron plasmas. *Plasma Sources, Sci. Technol.* **2**, 229–234.

Birdsall, C. K. and Langdon, A. B. 1991 *Plasma Physics via Computer Simulation*. Adam Hilger, Bristol.

Cooney, J. L., Aossey, D. W., Williams, J. E., Gavin, M. T., Kim, H. S., Hsu, Y. C., Scheller, A. and Lonngren, K. E. 1993 Observations on negative ion plasmas. *Plasma Sources, Sci. Technol.* **2**, 73–80.

Das, G. C. and Singh, K. I. 1991 Cylindrical and spherical solitons at the critical density of negative ions in a generalised multicomponent plasma. *Aust. J. Phys.* **44**, 523–533.

Donnelly, I. J. and Watterson, P. A. 1989 Ion-matrix sheath structure around cathodes of complex shape. *J. Phys. D: Appl. Phys.* **22**, 90–93.

El-Zein, Y., Amin, A., Shen, C., Yi, S., Lonngren, K. E. and Sheridan, T. E. 1996 Two dimensional sheath evolution in a negative ion plasma. *J. Appl. Phys.* **79**, 3853–3860.

El-Zein, Y., Yi, S., Lonngren, K. E., Alexeff, I., Sheridan, T. E. and Hsuan, H. 1997 Plasma sheath evolution from perturbed electrodes in a negative-ion plasma. *J. Plasma Phys.* **57**, 47–57.

Lim, W. B., Cooney, J., Ghaemi, M. S., Gavin, M., Andersen, D. R. and Lonngren, K. E. 1991 On plasma sheaths surrounding complex shapes as measured using ion acoustic waves. *J. Phys. D: Appl. Phys.* **24**, 1081–1085.

Sheridan, T. E. 1996*a* Particle-in-cell simulation of the pulsed sheath in a trench. *IEEE Trans. Plasma Sci.* **24**, 57–58.

Sheridan, T. E. 1996*b* Ion focusing by an expanding, two-dimensional plasma sheath. *Appl. Phys. Lett.* **68**, 1918–1920.

Sheridan, T. E. 1996*c* Self similar sheath expansion away from a segmented planar electrode. *Phys. Plasmas* **3**, 2461–2466.

Williams, J. E., Cooney, J. L., Aossey, D. W. and Lonngren, K. E. 1992 Cylindrical and spherical solitons in a positive ion–negative ion plasma. *Phys. Rev.* **A45**, 5897–5900.

Yi, S., Cooney, J. L., Kim, H. S., Amin, A., El-Zein, Y. and Lonngren, K. E. 1996 Reflection of modified Korteweg–de Vries solitons in a negative ion plasma. *Phys Plasmas* **3**, 529–535.

https://doi.org/10.1017/S0022377897006065 Published online by Cambridge University Press